GEOCHEMISTRY OF CORE SAMPLES OF THE TIVA CANYON TUFF FROM DRILL HOLE UE-25 NRG#3, YUCCA MOUNTAIN, NEVADA

by Zell E. Peterman and Kiyoto Futa

U.S. GEOLOGICAL SURVEY

Open-File Report 95-325

Prepared in cooperation with the
NEVADA OPERATIONS OFFICE,
U.S. DEPARTMENT OF ENERGY under
Interagency Agreement DE-AI08-92NV10874

Denver, Colorado
1996

U.S. DEPARTMENT OF THE INTERIOR

BRUCE BABBITT, Secretary

U.S. GEOLOGICAL SURVEY

Gordon P. Eaton, Director

For additional information write to:
Chief, Earth Science Investigations Program
Yucca Mountain Project Branch
U.S. Geological Survey
Box 25046, MS 421
Denver Federal Center
Denver, CO 80225

Copies of this report can be purchased from:
U.S. Geological Survey
Earth Science Information Center
Open-File Reports Section
Box 25286, MS 517
Denver Federal Center
Denver, CO 80225

CONTENTS

FIGURES

TABLES

CONVERSION FACTORS AND VERTICAL DATUM

Multiply	By	To obtain
foot (ft)	0.3048	meter
gram (g)	0.03527	ounce
inch (in.)	2.54	centimeter

The following term also is used in this report: parts per million (ppm)

Sea level: In this report "sea level" refers to the National Geodetic Vertical Datum of 1929 (NGVD of 1929)—a geodetic datum derived from a general adjustment of the first-order level nets of both the United States and Canada, formerly called Sea Level Datum of 1929.

Geochemistry of Core Samples of the Tiva Canyon Tuff from Drill Hole UE-25 NRG#3, Yucca Mountain, Nevada

By Zell E. Peterman *and* Kiyoto Futa

Abstract

The Tiva Canyon Tuff of Miocene age is composed of crystal-poor, high-silica rhyolite overlain by a crystal-rich zone that is gradational in composition from high-silica rhyolite to quartz latite. Each of these zones is divided into subzones that have distinctive physical, mineralogical, and geochemical features. Accurate identification of these subzones and their contacts is essential for detailed mapping and correlation both at the surface and in the subsurface in drill holes and in the exploratory studies facility (ESF). This report presents analyses of potassium (K), calcium (Ca), titanium (Ti), rubidium (Rb), strontium (Sr), yttrium (Y), zirconium (Zr), niobium (Nb), barium (Ba), lanthanum (La), and cerium (Ce) in core samples of the Tiva Canyon Tuff from drill hole UE-25 NRG#3. The concentrations of most of these elements are remarkably constant throughout the high-silica rhyolite, but at its upper contact with the crystal-rich zone, Ti, Zr, Ba, Ca, Sr, La, Ce, and K begin to increase progressively through the crystal-rich zone. In contrast, Rb and Nb decrease, and Y remains essentially constant. Initial $^{87}Sr/^{86}Sr$ ratios are relatively uniform in the high-silica rhyolite with a mean value of 0.7117, whereas initial $^{87}Sr/^{86}Sr$ ratios decrease upward in the quartz latite to values as low as 0.7090.

INTRODUCTION

Yucca Mountain (fig. 1) is being evaluated for its suitability as a site for a potential high-level nuclear-waste repository (U.S. Department of Energy, 1988). The U.S. Geological Survey (USGS) is conducting site characterization studies for the Department of Energy Yucca Mountain Site Characterization Project under Interagency Agreement No. DE-AI08-92NV10874. These studies include detailed petrographic, geochemical, and isotopic analyses of samples of the volcanic rock units collected from drill cores and from outcrops to aid in the identification and lateral correlation of zonal features. This report presents geochemical and isotopic data obtained on core samples of the Tiva Canyon Tuff from drill hole UE-25 NRG#3 (hereafter referred to as NRG#3). This drill hole is located west of Exile Hill (fig. 1) at an altitude of 3,823 ft at 36°51'18" N and 116°25'59" W (Nevada State coordinates 766,251 N and 568,316 E). The drill hole has a plunge of 56.5° on an azimuth of 95.2°. The total length of the drill hole is 330 ft. Geslin and others (1995) described the lithology and zonal features of the core, and their zonal designations are used in this report (table 1).

Purpose and Scope

The purpose of this study is to document the geochemical variations in the Tiva Canyon Tuff using energy-dispersive X-ray fluorescence analyses of selected elements (K, Ca, Ti, Rb, Sr, Y, Zr, Nb, Ba, La, and Ce). Drill hole NRG#3 was selected because it intercepted a relatively complete section of the crystal-rich zone, which is difficult to obtain in outcrop in a single section. Forty-nine samples of core from drill hole NRG#3 were obtained for analyses. Sample spacing was designed to be representative of the main lithologic zones of the moderately and densely welded portions of the unit and to closely delineate the contact between the high-silica rhyolite and the transitional quartz latite.

Acknowledgments

The authors gratefully acknowledge the careful reviews by Dr. Thomas C. Moyer and Ms. Frances Singer (SAIC, Science Applications International). Samples of core from drill hole NRG#3 were carefully

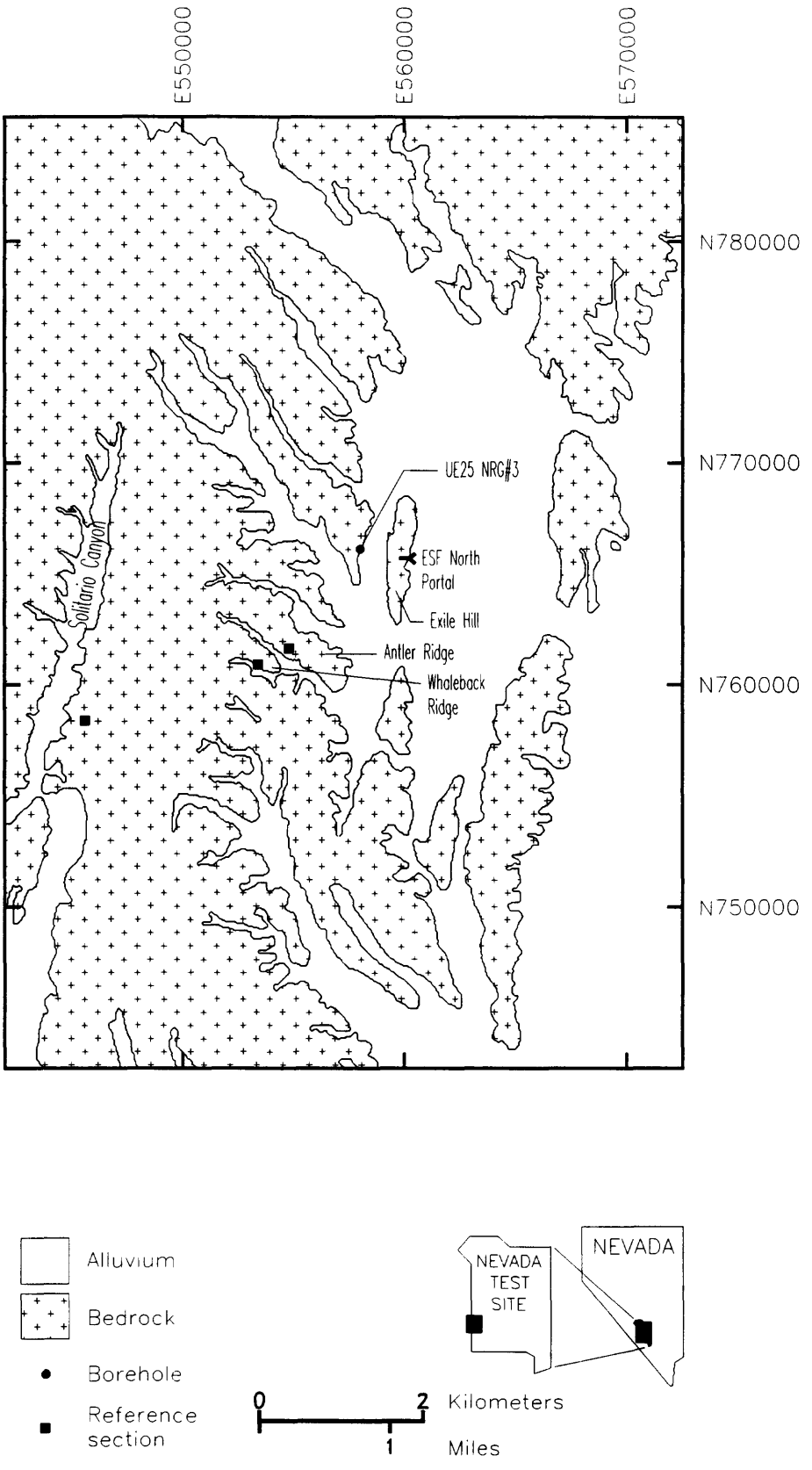

Figure 1. Location of drill hole UE-25 NRG#3 and selected geographic features. The grid is the Nevada State Coordinate System.

Table 1. Lithostratigraphic zonation of the Tiva Canyon Tuff in drill hole UE-25 NRG#3 at Yucca Mountain, Nevada

[Depth, distance along the drill hole; Stratigraphic interval, true stratigraphic thickness; ft, feet]

Depth (ft)	Stratigraphic interval (ft)	Zone	Subzone
0–12.0	0–8.2	CRYSTAL-RICH NONLITHOPHYSAL ZONE (Tpcrn)	Pumice-poor subzone (Tpcrn3)
12.0–82.0	8.2–54.8		Mixed pumice subzone (Tpcrn2)
82.0–100.0	54.8–66.8		Crystal transition subzone (Tpcrn1)
100.0–188.0	66.8–125.6	CRYSTAL-POOR UPPER LITHOPHYSAL ZONE (Tpcpul)	
188.0–200.0	125.6–133.6		Spherulite-rich subzone (Tpcpul1)
200.0–206.7	133.6–138.1		
206.7–268.2	138.1–179.2	CRYSTAL-POOR MIDDLE NONLITHOPHYSAL ZONE (Tpcpmn)	
268.2–330.0	179.2–220.4	CRYSTAL-POOR LOWER LITHOPHYSAL ZONE (Tpcpll)	

selected by Beth Widmann (SAIC) and April Walker (USGS). Duane Craft and Shannon Mahan (USGS) provided outstanding technical support in sample preparation and X-ray fluorescence analyses, respectively.

STUDY METHODS

Pieces of core approximately 3 in. long were split, and one-half was retained for reference in the Sample Management Facility at Jackass Flats near Yucca Mountain. The other one-half core was sampled, using a 0.5-in-diameter diamond drill, to obtain two or three subsample cores approximately 1 to 1.5 in. long with emphasis on the rock matrix; lithic clasts and large pumice clasts were avoided as much as possible. These subsample cores were cleaned in distilled water, dried, and then pulverized to 200-mesh powder in a hardened steel shatterbox. A representative split of approximately 3 to 5 g of the 200-mesh rock powder was then analyzed for selected major and trace elements using a multi-target, energy-dispersive, X-ray fluorescence spectrometer. The USGS standard GSP-1 was analyzed with each set of 16 samples; the following coefficients of variation for the analyzed elements were obtained: K, ±1.2 percent; Ca, ±3.7 percent; Ti, ±2.4 percent; Rb, ±1.4 percent; Sr, ±1.3 percent; Y, ±8.3 percent; Zr, ±3.6 percent; Nb, ±3.7 percent; Ba, ±2.9 percent; La, ±7.1 percent; and Ce, ±3.9 percent.

For the isotopic analyses, strontium was extracted from a split of the 200-mesh powder by digestion in concentrated HF and H_2SO_4. Strontium was purified by conventional ion-exchange chromatography, and isotope ratios were determined on a Finnigan MAT 262 thermal ionization mass spectrometer operating in a fully automatic static mode. Two samples of the USGS carbonate standard EN-1 were analyzed in each magazine of 15 samples. The mean $^{87}Sr/^{86}Sr$ of standard EN-1 was 0.70911 ±0.00001 during the course of the analyses of the NRG#3 samples. Mass fractionation during isotopic analyses was eliminated by normalizing the measured $^{86}Sr/^{88}Sr$ ratios to a value of 0.1194 and adjusting the $^{87}Sr/^{86}Sr$ ratios accordingly. The normalized $^{87}Sr/^{86}Sr$ values then were adjusted to a scale on which the value for standard EN-1 is 0.70920. Standard EN-1 was prepared from the shell of a modern *Tridacna* collected from Enewetok Lagoon in the western Pacific Ocean. Its contained Sr has the isotopic composition of ocean water. Uncertainties in the normalized and adjusted $^{87}Sr/^{86}Sr$ are better than ±0.01 percent at the 95-percent confidence level.

LITHOSTRATIGRAPHIC AND CHEMOSTRATIGRAPHIC FRAMEWORK

The Tiva Canyon Tuff, the uppermost densely welded tuff of the Paintbrush Group of Miocene age, crops out extensively at Yucca Mountain (Scott and Bonk, 1984). The underlying, compositionally similar, but much thicker, Topopah Spring Tuff will be the host rock for construction of the potential repository. The Tiva Canyon and Topopah Spring Tuffs are internally zoned in their physical and chemical attributes including major and trace element composition, mineralogy, phenocryst type and content, degree of welding, and

distribution of lithophysal cavities, pumice clasts, and lithic clasts (Lipman and others, 1966; Schuraytz and Vogel, 1989; Flood and others, 1989; Broxton and others, 1989; Farmer and others, 1991; Peterman and others, 1991; Singer and others, 1994). In both the Tiva Canyon and Topopah Spring Tuffs, crystal-poor high-silica rhyolite is overlain by crystal-rich rocks that are transitional in composition from high-silica rhyolite to quartz latite at the top of the unit (Flood and others, 1989; Schuraytz and Vogel, 1989). These compositional zones reflect gradients in the source magma that developed through crystal settling prior to eruption of the ash flows (Lipman and others, 1966; Smith, 1979), although the original magmatic compositions undoubtedly have been modified by eruptive, depositional, and post-depositional processes (Cas and Wright, 1993). Systematic Sr isotopic differences between the high-silica rhyolite and the quartz latite, and isotopic disequilibrium between phenocrysts and ground mass indicated that isotopic gradients (Noble and Hedge, 1969) accompanied the chemical zonations in the magma chambers (Lipman and others, 1966). More recent studies have shown similar neodymium (Nd) and lead (Pb) isotopic variations (Hildreth, 1981; Johnson, 1989; Tegtmeyer and Farmer, 1990; Farmer and others, 1991). The isotopic zonation and the presence of older zircon in some tuffs indicate that assimilation of country rock as well as crystal settling produced the compositional gradients in the magmas (Johnson, 1989; Tegtmeyer and Farmer, 1990).

Reference sections have been established at Antler Ridge, Whaleback Ridge, and Solitario Canyon (fig. 1) to characterize the internal zonation of the Tiva Canyon Tuff on the basis of petrography and geochemistry and to correlate these features with the physical and mineralogical zonations used in outcrop mapping (Scott and Bonk, 1984). Chemical analyses have been completed on samples from these reference sections (USGS, unpub. data), and composite geochemical profiles are shown in figure 2. The profiles were constructed by normalizing the stratigraphic positions of the samples to the contact between the crystal-rich and crystal-poor zones. Concentrations of most of the analyzed elements are uniform in the high-silica rhyolite (crystal-poor zone) as exemplified by Ba, Zr, and Ti (fig. 2). Rb displays considerably more scatter, which is probably the consequence of alkali-element mobility during late stage alteration and devitrification (Lipman, 1965). The elements Zr and Ti are remarkably uniform in the high-silica rhyolite with a variability that is commensurate solely with analytical uncertainty. The distribution of Ba shows more dispersion than Ti and Zr but is essentially invariant through the high-silica rhyolite. Rubidium displays considerable scatter in the high-silica rhyolite with a significant depletion in the lower part of the unit at the Solitario Canyon reference section. This zone also shows enrichment in ^{18}O, which Marshall and others (in press) attribute to isotopic exchange attendant with hydration of the volcanic glass.

An important geochemical feature of the Tiva Canyon Tuff is the change in the pattern of element variation at the contact between the crystal-poor upper lithophysal zone and the superjacent crystal transition subzone (table 1, fig. 2). Above this contact, Ti, Zr, and Ba increase progressively upward through the crystal-rich zone (fig. 2). The elements La, Ce, Ca, Sr, and K (not shown) also increase upward in this zone. The decrease in Rb upward (fig. 2) with the concomitant rise in K results in a systematic increase in K/Rb ratios through the crystal-rich zone. For the Antler Ridge section, lines fit to the geochemical trends within the crystal-poor and crystal-rich zones intersect within 1 to 3 feet of the physical contact (Singer and others, 1994).

In outcrop, the crystal transition subzone corresponds in part to the lower part of the upper cliff map zone of Scott and Bonk (1984) which can be distinguished mineralogically from the subjacent high-silica rhyolite by the first appearance of biotite and plagioclase phenocrysts in the groundmass (Singer and others, 1994). The compositional gradation from high-silica rhyolite to quartz latite through much of the crystal-rich zone poses nomenclature problems in the assignment of specific rock names. Flood and others (1989), following Byers and others (1976), used the terms high-silica rhyolite for the crystal-poor zone and rhyolite and quartz latite for the crystal-rich zone. Using the representative analyses of Flood and others (1989) and trace element analyses of outcrop samples from the crystal-rich zone, Marshall and others (in press) concluded that the true quartz latite is characterized by Ba contents of 1,500 ppm or greater. Using this criterion, only the uppermost 9 to 12 ft of the NRG#3 section is quartz latite. Thus, all of the crystal transition zone and most of the pumice-poor subzone (table 1) are composed of the compositionally transitional rock types. The following rock terms will be used for convenience in the ensuing discussions:

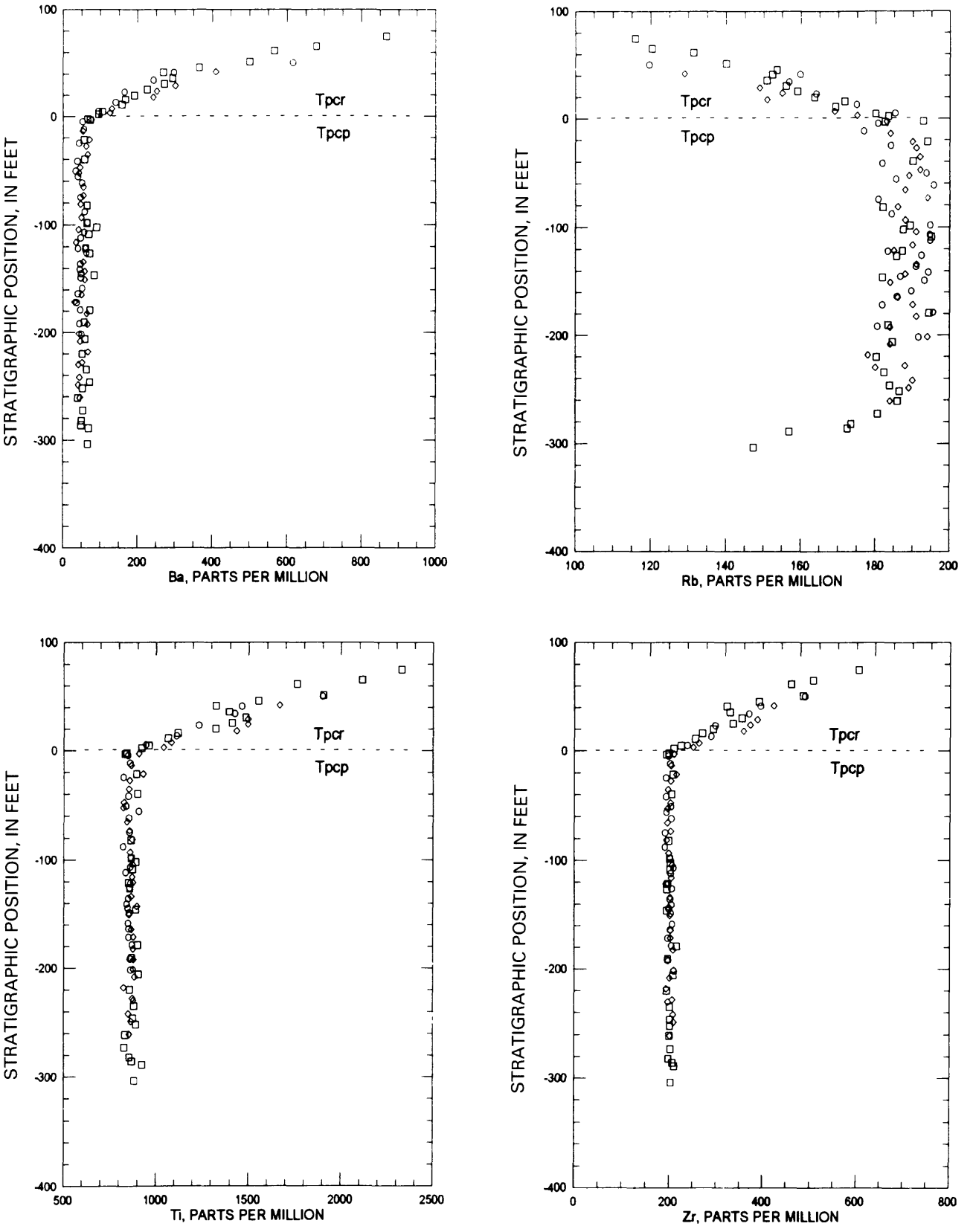

Figure 2. Composite geochemical profiles for samples from the Antler Ridge (circles), Whaleback Ridge (diamonds), and Solitario Canyon (squares) reference sections. (See table 2, footnote 2 for explanation of nomenclature.)

(1) high-silica rhyolite (all of the crystal-poor zone), (2) transitional quartz latite (crystal transition and mixed pumice subzones), and (3) quartz latite (pumice-poor subzone).

GEOCHEMISTRY OF CORE SAMPLES FROM UE-25 NRG#3

Geochemical and Sr isotopic data for the Tiva Canyon Tuff intersected in drill hole UE-25 NRG#3 are presented in table 2. Sample locations are given as positions along the axis of the drill hole and in true stratigraphic position relative to the collar of the drill hole. Stratigraphic positions (table 2) were calculated on the basis of the strike of beds of 022° and a southeasterly dip of 15° (D. Buesch, U.S. Geological Survey, written commun., 1994; Buesch and others, 1994) and by adjusting for the plunge and strike of the borehole (56.5° at azimuth of 95.2°). The attitude of the bedding at the NRG#3 drill pad is consistent with measurements made underground in the ESF of 018° strike and 15° SE dip (Steve Beason, U.S. Bureau of Reclamation, oral commun., April 19, 1995). The zonal contacts identified along the borehole by Geslin and others (1995) were mathematically transposed to intercepts along the vertical and then converted to stratigraphic position based on the 15° dip of the unit.

The remarkable uniformity of the high-silica rhyolite of the crystal-poor zone is illustrated by the means and standard deviations of elemental concentrations in the reference sections (table 3). Only in the lower vitric part of the unit have the compositions been modified significantly by post-depositional processes (fig. 2). Except for Ba and Ca, mean element contents of the high-silica rhyolite in NRG#3 (71.1 to 217.2 ft) are in agreement with the mean compositions of the reference sections (table 3). Zirconium and Ti are typically uniform throughout this unit in NRG#3, but Ba is lower in most of high-silica rhyolite than in the reference sections, reaching comparable values only in the upper 30 ft of the unit as shown by the inset in figure 3. The stratigraphically lowest sample in the crystal-rich zone (66.8 ft, table 2) has significantly more Ba (89 ppm) than the highest sample (71.1 ft) in the crystal-poor zone (54 ppm). In the reference sections, Ba increases systematically and progressively upward from this contact (fig. 2), whereas Ba in NRG#3 decreases at 64.7 ft and then increases upward but with some minor reversals in trend (inset, fig. 3). Titanium and Zr also show similar reversals a few feet above the contact between the crystal-poor and crystal-rich zones.

Except for some scatter in the lower part of the unit, Ca is relatively uniform throughout most of the high-silica rhyolite and increases progressively upward through the transitional quartz latite without notable reversals in trend (fig. 4). In the upper lithophysal subzone of the high-silica rhyolite, a linear increase in the middle part of the subzone is followed by a decrease in Sr up to the contact between crystal-poor and crystal-rich zones. In contrast to Ca, Sr displays systematic differences in concentrations among the lithostratigraphic zones of the high-silica rhyolite. Strontium appears to decrease in a stepwise fashion from the lower lithophysal, through the middle nonlithophysal to the upper lithophysal zones as illustrated by means and standard deviations of 30.6±3.3 ppm, 23.0±3.6 ppm, and 19.2±2.0 ppm, respectively (fig. 5). Immediately above the crystal-rich contact, Sr decreases and then increases systematically through the transitional quartz latite.

The rare-earth elements La and Ce, scatter excessively throughout the high-silica rhyolite overall but define no particular trend throughout the unit (fig. 6). Both elements increase progressively upward through the crystal-rich zone. Cerium especially shows considerable scatter in the crystal transition subzone (Tpcrn1, fig. 6). The scatter of these elements in both the crystal-poor and crystal-rich zones is attributed to the fact that they are largely sequestered in trace accessory minerals such as allanite, perrierite, and sphene. Much larger subsamples of the tuff would likely reduce the scatter in these elements because the trace accessory minerals would be more adequately represented.

In contrast with most of the other elements, relatively uniform concentrations of Nb and Rb in the high-silica rhyolite are followed by decreases upward through the crystal-rich zone (fig. 7). Although generally decreasing, Rb shows appreciable scatter through crystal transition subzone (Tpcrn1, fig. 7) with no clear break in trend at the lower contact. The scatter of Rb in NRG#3 is consistent with similar scatter observed in the reference sections (fig. 3), which in part derives from late-stage alkali mobility.

A decoupling of the alkalies K and Rb occurs in the crystal-rich zone where K increases markedly upward (fig. 8) whereas Rb decreases over the same stratigraphic interval. K and Rb are coherent in the high-silica rhyolite as shown by the nearly uniform K/Rb ratios throughout the unit (fig. 9). Throughout

Table 2. Geochemical and isotopic data for core samples from drill hole UE-25 NRG#3, Yucca Mountain, Nevada

[ft, feet; %, percent; ppm, parts per million; IR (Sr), initial $^{87}Sr/^{86}Sr$ ratio; ---, no analyses were done]

Sample ID[1]	Zone[2]	Depth (ft)	Strat.[3] (ft)	K (%)	Ca (%)	Ti (%)	Rb (ppm)	Sr (ppm)	Y (ppm)	Zr (ppm)	Nb (ppm)	Ba (ppm)	La (ppm)	Ce (ppm)	$^{87}Rb/^{86}Sr$	$^{87}Sr/^{86}Sr$	IR (Sr)
30105	Tpcrn3	8.4–8.5	5.6	4.97	0.832	3157	86	199	40	785	12	2289	223	394	1.25	0.70922	0.70899
29772	Tpcrn2	13.4–13.7	9.1	4.97	0.787	3004	89	194	39	763	13	2182	232	388	---	---	---
29773	Tpcrn2	19.1–19.4	12.9	4.66	0.653	2642	98	104	41	637	16	1058	191	314	2.73	0.71022	0.70973
29774	Tpcrn2	24.2–24.5	16.3	4.71	0.506	2513	108	106	40	613	15	1090	196	322	---	---	---
29775	Tpcrn2	36.9–37.1	24.7	4.63	0.526	2386	112	99	40	611	18	868	186	308	---	---	---
29776	Tpcrn2	42.3–42.6	28.4	4.73	0.472	2328	120	96	42	576	18	794	175	294	3.62	0.71085	0.71020
29777	Tpcrn2	48.6–48.9	32.8	4.43	0.442	1928	142	68	40	488	19	567	159	252	6.04	0.71140	0.71031
29778	Tpcrn2	54.9–55.3	36.8	4.42	0.467	1897	131	67	44	500	20	533	150	243	---	---	---
29779	Tpcrn1	82.0–82.3	54.9	3.93	0.352	1338	163	59	41	342	25	490	92	163	8.00	0.71208	0.71064
29780	Tpcrn1	86.3–86.5	57.7	3.94	0.324	1336	160	44	43	331	25	231	92	141	10.53	0.71306	0.71116
35121	Tpcrn1	88.5–88.7	59.2	3.77	0.289	1027	194	33	42	249	32	110	53	73	---	---	---
29781	Tpcrn1	88.8–89.0	59.4	3.67	0.225	1026	189	33	43	243	32	103	48	83	16.58	0.71492	0.71193
35122	Tpcrn1	89.0–89.4	59.6	3.59	0.247	1033	171	36	39	239	32	143	57	96	---	---	---
36237	Tpcrn1	89.7–89.9	60.0	3.67	0.235	1065	186	35	37	258	28	136	46	87	---	---	---
35123	Tpcrn1	91.8–92.0	61.4	3.55	0.204	967	184	25	43	229	30	94	46	79	---	---	---
30106	Tpcrn1	92.2–92.5	61.7	3.60	0.195	968	186	28	40	227	29	80	45	78	19.23	0.71533	0.71186
36236	Tpcrn1	93.7–93.8	62.6	3.55	0.205	897	191	24	36	223	29	89	42	70	---	---	---
35124	Tpcrn1	96.0–96.3	64.2	3.51	0.175	833	182	15	39	200	29	58	42	73	---	---	---
35125	Tpcrn1	96.8–96.9	64.7	3.47	0.177	885	185	16	35	198	31	67	46	83	---	---	---
29782	Tpcrn1	99.6–99.9	66.6	3.58	0.165	866	189	18	43	205	31	44	35	64	30.41	0.71715	0.71166
35126	Tpcrn1	99.9–100.2	66.8	3.48	0.165	877	189	20	36	197	32	89	45	72	---	---	---
29783	Tpcpul	106.4–106.6	71.1	3.55	0.169	881	186	17	45	211	34	54	47	74	31.69	0.71722	0.71150
29784	Tpcpul	115.2–115.5	77.1	3.61	0.174	900	188	16	38	207	31	44	43	61	---	---	---
29785	Tpcpul	123.7–124.0	82.7	3.62	0.199	872	188	22	36	206	30	54	49	98	---	---	---
29786	Tpcpul	138.5–138.9	92.7	3.63	0.188	883	195	20	34	225	31	42	33	91	---	---	---
29787	Tpcpul	145.0–145.3	97.0	3.54	0.181	895	196	20	42	214	31	42	35	50	28.38	0.71669	0.71157
29788	Tpcpul	152.4–152.7	103.6	3.58	0.178	859	200	21	38	204	31	19	38	57	---	---	---
29789	Tpcpul	160.0–160.3	107.0	3.54	0.173	879	191	19	60	198	32	24	40	61	---	---	---
30110	Tpcpul	177.9–178.2	118.9	3.57	0.161	853	189	17	40	198	32	23	41	70	---	---	---
29790	Tpcpul	185.1–185.4	123.7	3.79	0.177	846	192	21	42	202	32	35	37	67	---	---	---
29791	Tpcpul	192.5–192.8	128.7	3.71	0.180	858	188	17	38	198	32	19	39	69	32.03	0.71757	0.71179
30107	Tpcpul	203.3–203.6	135.9	3.63	0.175	830	189	17	37	194	31	31	52	75	---	---	---
29792	Tpcpmn	206.9–207.3	138.3	3.60	0.177	835	190	16	39	202	33	20	38	74	---	---	---
29793	Tpcpmn	212.9–213.1	142.3	3.57	0.181	867	193	25	42	204	38	28	56	74	---	---	---
29794	Tpcpmn	220.1–220.4	147.1	3.61	0.171	866	197	24	40	197	32	24	37	69	---	---	---
29795	Tpcpmn	227.6–227.9	152.1	3.58	0.176	871	189	22	48	200	32	33	56	62	---	---	---

Table 2. Geochemical and isotopic data for core samples from drill hole UE-25 NRG#3, Yucca Mountain, Nevada--Continued

Sample ID[1]	Zone[2]	Depth (ft)	Strat.[3] (ft)	K (%)	Ca (%)	Ti (%)	Rb (ppm)	Sr (ppm)	Y (ppm)	Zr (ppm)	Nb (ppm)	Ba (ppm)	La (ppm)	Ce (ppm)	$^{87}Rb/^{86}Sr$	$^{87}Sr/^{86}Sr$	IR (Sr)
29796	Tpcpmn	235.4–235.9	157.4	3.62	0.186	873	194	23	38	203	34	25	37	80	---	---	---
29797	Tpcpmn	243.9–244.2	163.0	3.56	0.167	894	192	22	46	211	33	26	44	59	---	---	---
29798	Tpcpmn	253.3–253.4	169.2	3.60	0.163	866	193	25	41	204	32	32	42	80	---	---	---
29799	Tpcpmn	260.3–260.6	174.0	3.63	0.167	875	193	20	48	201	33	23	53	68	27.94	0.71651	0.71147
30108	Tpcpmn	267.1–267.4	178.5	3.63	0.187	884	189	30	42	201	33	23	45	65	---	---	---
29800	Tpcpll	274.5–274.5	183.5	3.63	0.171	885	190	34	38	204	32	28	45	61	---	---	---
29801	Tpcpll	280.3–280.6	187.3	3.61	0.173	868	192	30	38	202	33	24	37	74	---	---	---
29802	Tpcpll	286.2–286.5	191.3	3.57	0.177	868	185	27	38	201	31	24	49	75	---	---	---
30111	Tpcpll	293.0–293.2	195.8	3.57	0.240	872	186	26	40	203	32	25	41	74	---	---	---
30109	Tpcpll	300.0–300.3	200.5	3.59	0.175	883	190	31	31	204	34	27	30	70	---	---	---
29803	Tpcpll	310.2–310.5	207.3	3.56	0.216	898	189	30	39	200	31	26	42	77	---	---	---
29804	Tpcpll	321.4–321.7	214.8	3.58	0.165	863	191	27	37	200	31	29	46	74	---	---	---
29805	Tpcpll	325.1–325.3	217.2	3.59	0.172	881	192	35	42	205	32	23	38	76	15.88	0.71516	0.71229

[1]Sample ID: These are the last five digits of the bar-code numbers, which are prefixed by SPC000.

[2]Zones: Tpc refers to Tertiary, Paintbrush Canyon Group, Tiva Canyon Tuff. Suffix letters identify internal zonal features: rn3, pumice-poor subzone of the crystal-rich nonlithophysal zone; rn2, mixed pumice subzone of the crystal-rich nonlithophysal zone; rn1, crystal transition subzone of the crystal-rich nonlithophysal zone; pul, crystal-poor upper lithophysal zone; pmn, crystal-poor middle nonlithophysal zone; and pll, crystal-poor lower lithophysal zone.

[3]Strat.: Designates the true stratigraphic position of the sample, taking into account the strike and dip of the unit and the plunge and azimuth of the borehole. The stratigraphic position is calculated from midpoint of the core sample interval.

Table 3. Mean compositions of the high-silica rhyolite of the Tiva Canyon Tuff, Yucca Mountain, Nevada

[n, number of analyses used to determine the mean and standard deviation (sigma); %, percent; ppm, parts per million]

Element	Reference section							
	Solitario Canyon n = 24		Whaleback Ridge n = 26		Antler Ridge n = 25		UE-25 NRG#3 n = 29	
	Mean	Sigma	Mean	Sigma	Mean	Sigma	Mean	Sigma
K (%)	3.60	0.17	3.56	0.04	3.63	0.08	3.60	0.05
Ca (%)	0.41	0.20	0.50	0.26	0.66	0.26	0.18	0.02
Ti (ppm)	870	24	863	17.8	853	16.0	872	16.6
Rb (ppm)	187	4.6	188	3.9	188	5.6	191	3.3
Sr (ppm)	17	4.2	19	5.1	19	4.2	24	5.7
Y (ppm)	39	1.8	42	4.7	44	3.4	41	5.2
Zr (ppm)	202	5.2	202	4.5	201	5.5	204	5.8
Nb (ppm)	32	1.3	32	1.1	31	1.0	32	1.5
Ba (ppm)	64	11.3	51	9.9	48	8.1	30	9.4
La (ppm)	47	5.3	43	5.3	43	5.5	42	6.7
Ce (ppm)	77	5.6	73	6.8	74	6.5	71	9.4

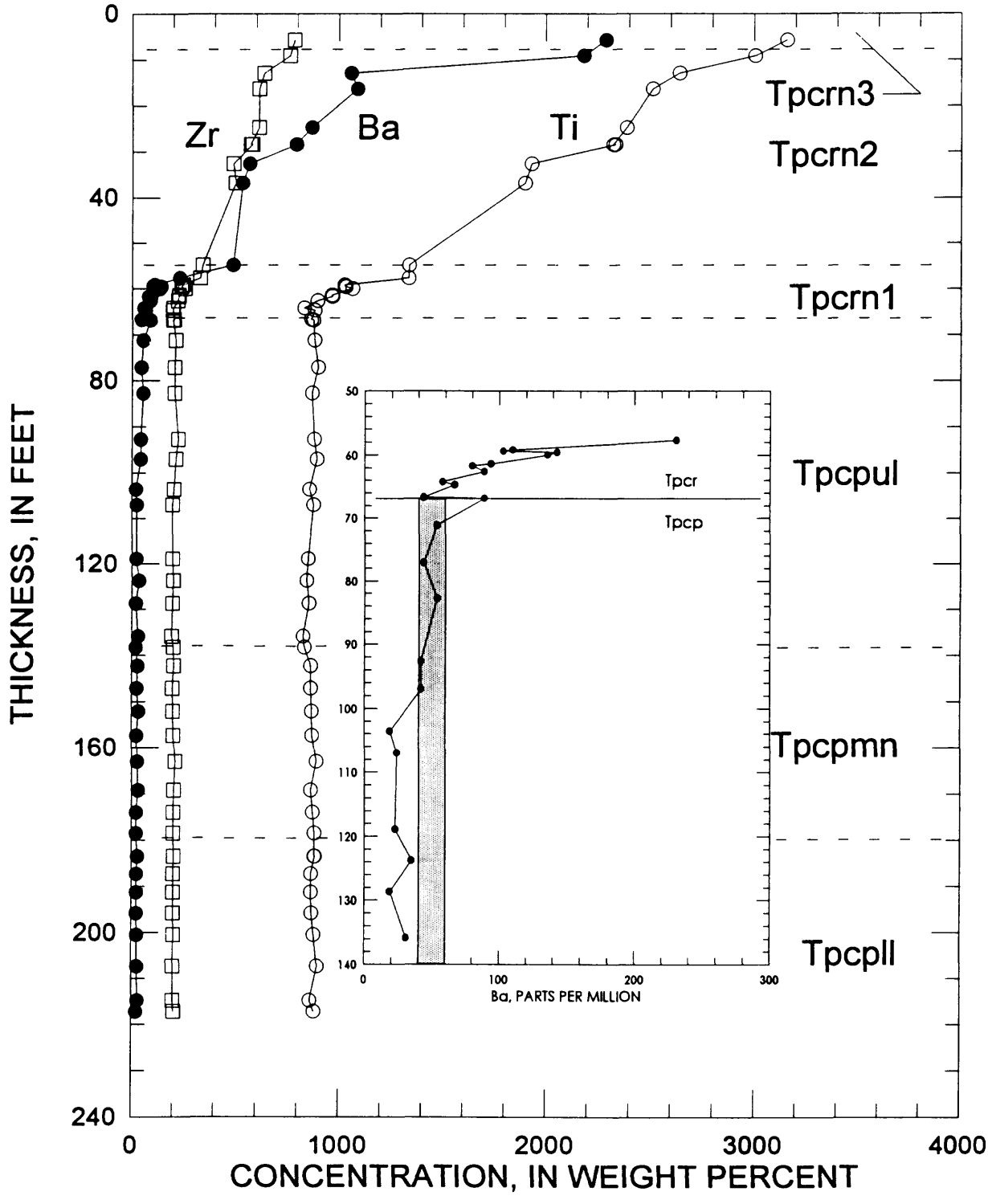

Figure 3. Concentrations of Ti, Zr, and Ba in samples of the Tiva Canyon Tuff from drill hole UE-25 NRG#3. The inset shows the distribution of Ba in the upper part of the crystal-poor zone and the lower part of the crystal-rich zone. The shaded vertical rectangle represents the mean concentration of Ba in the reference sections; the width is approximately defined by two standard deviations (table 3).

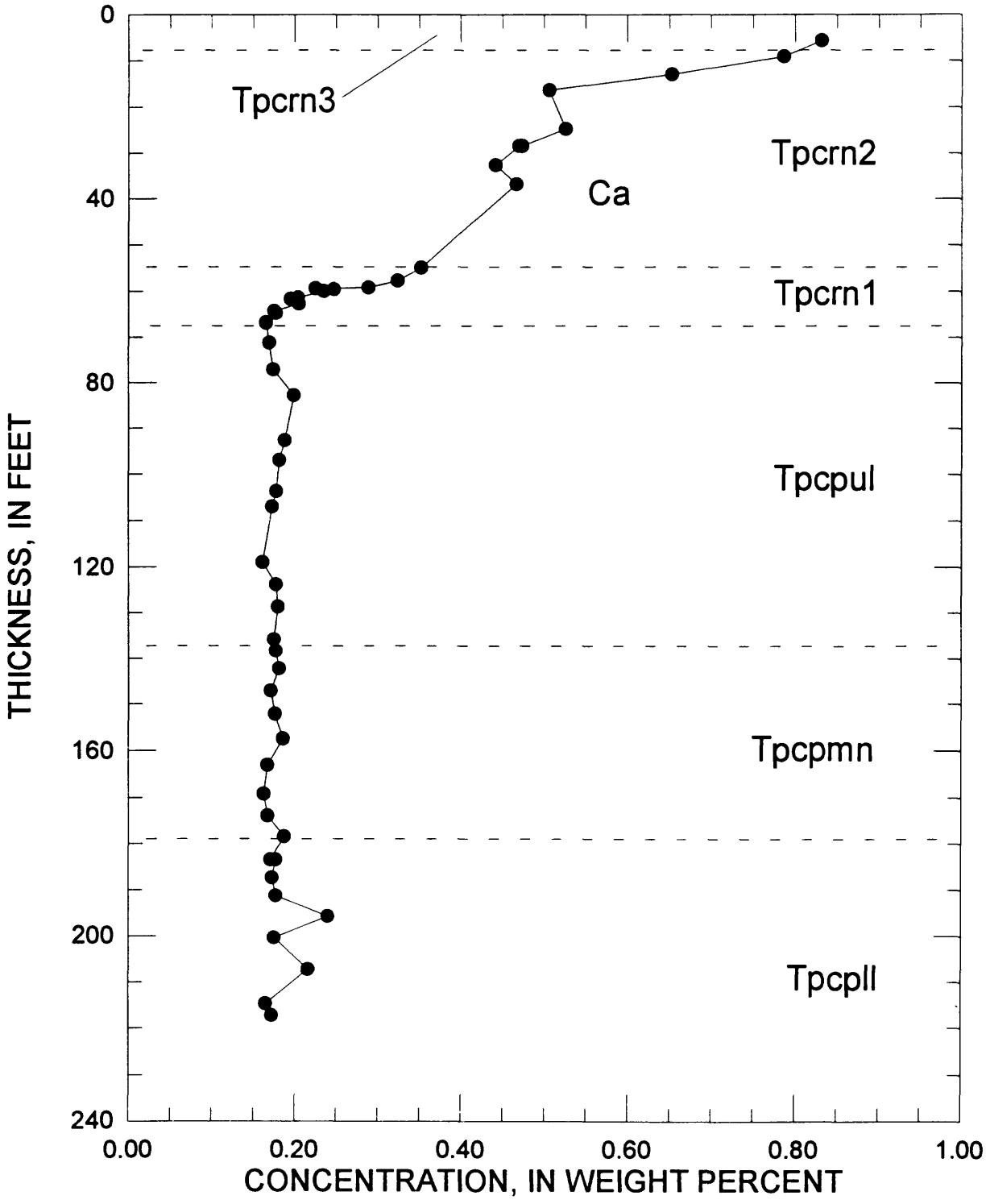

Figure 4. Concentration of Ca in samples of the Tiva Canyon Tuff from drill hole UE-25 NRG#3.

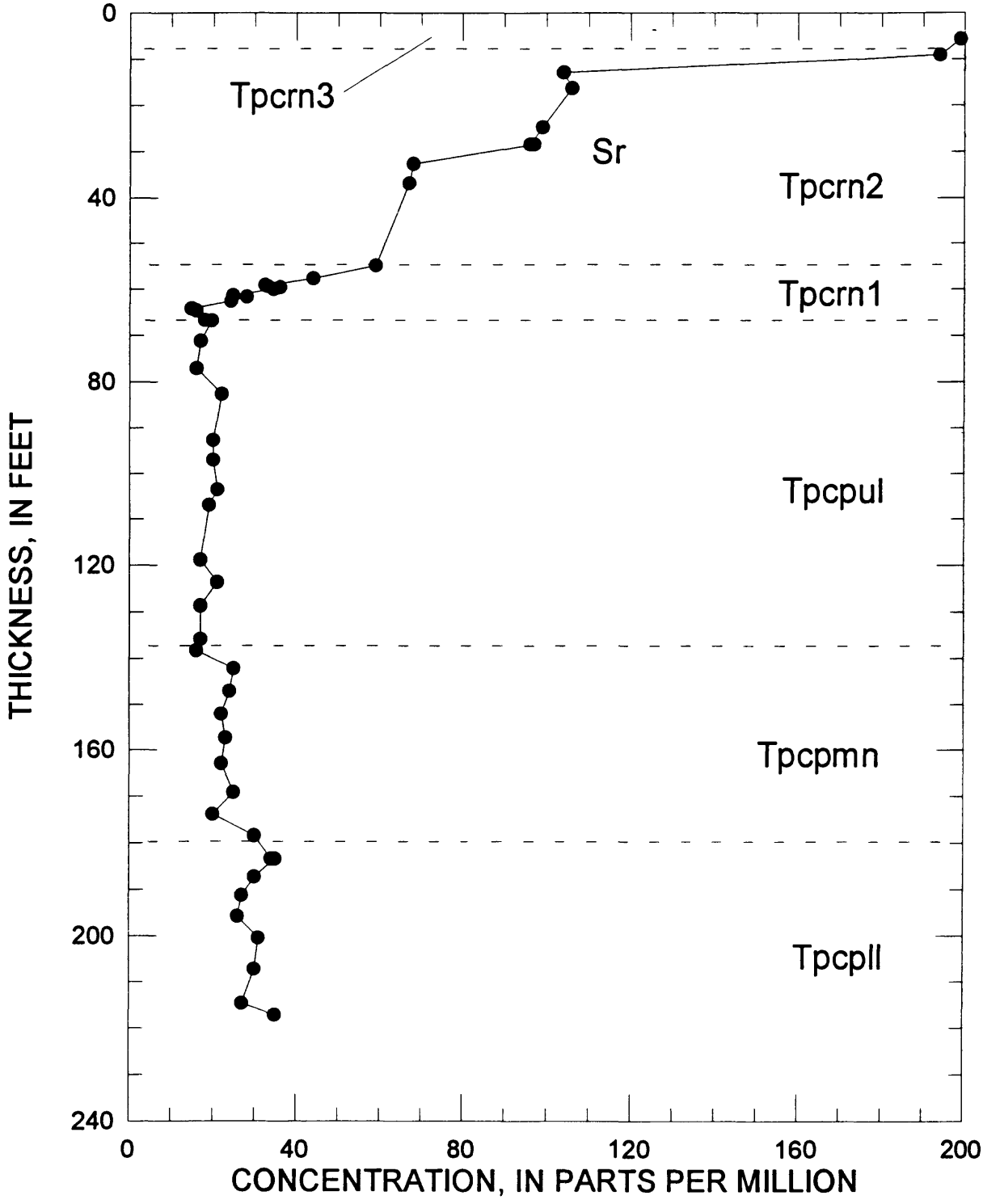

Figure 5. Concentration of Sr in samples of the Tiva Canyon Tuff from drill hole UE-25 NRG#3.

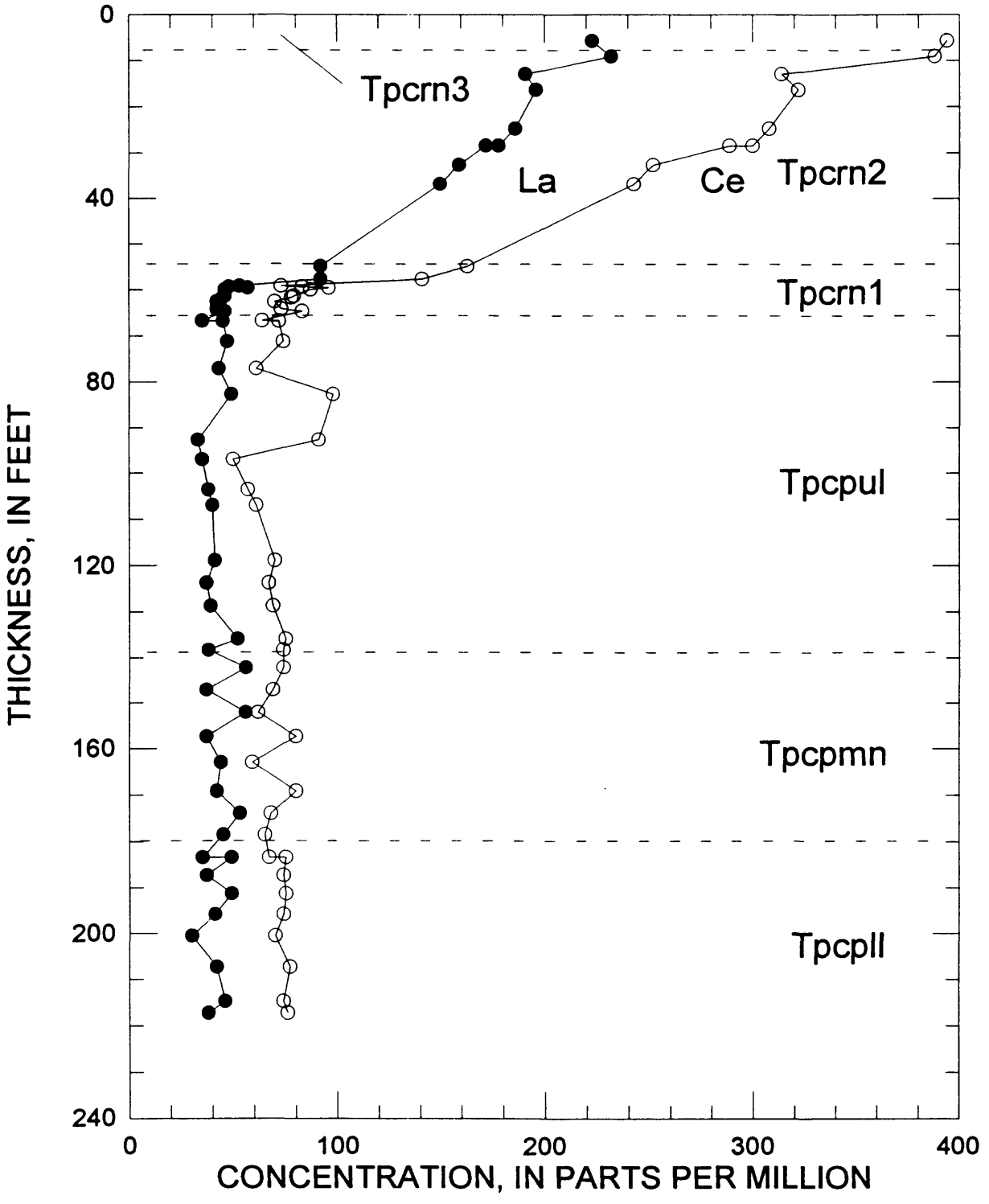

Figure 6. Concentrations of La and Ce in samples of the Tiva Canyon Tuff from drill hole UE-25 NRG#3.

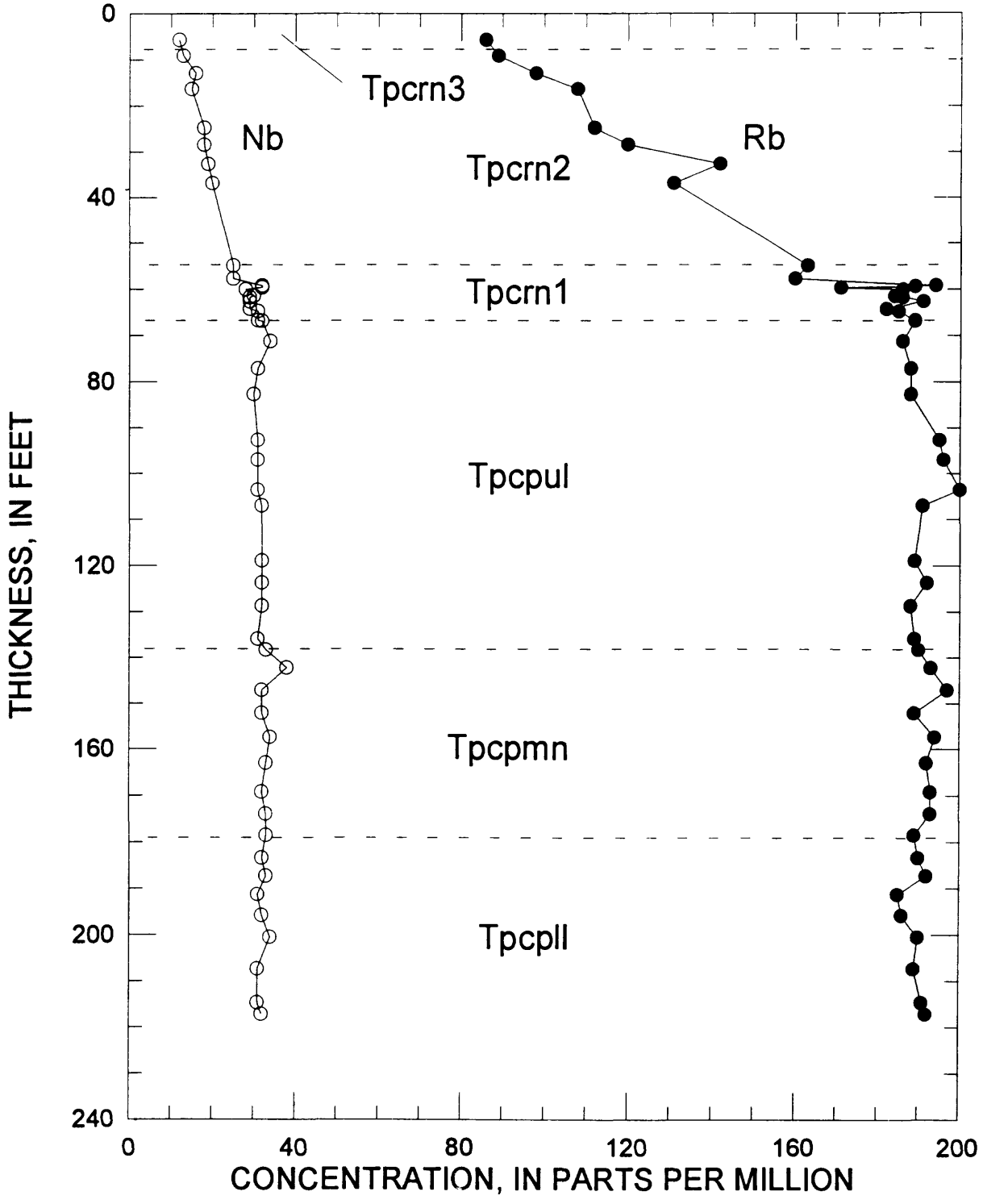

Figure 7. Concentrations of Nb and Rb in samples of the Tiva Canyon Tuff from drill hole UE-25 NRG#3.

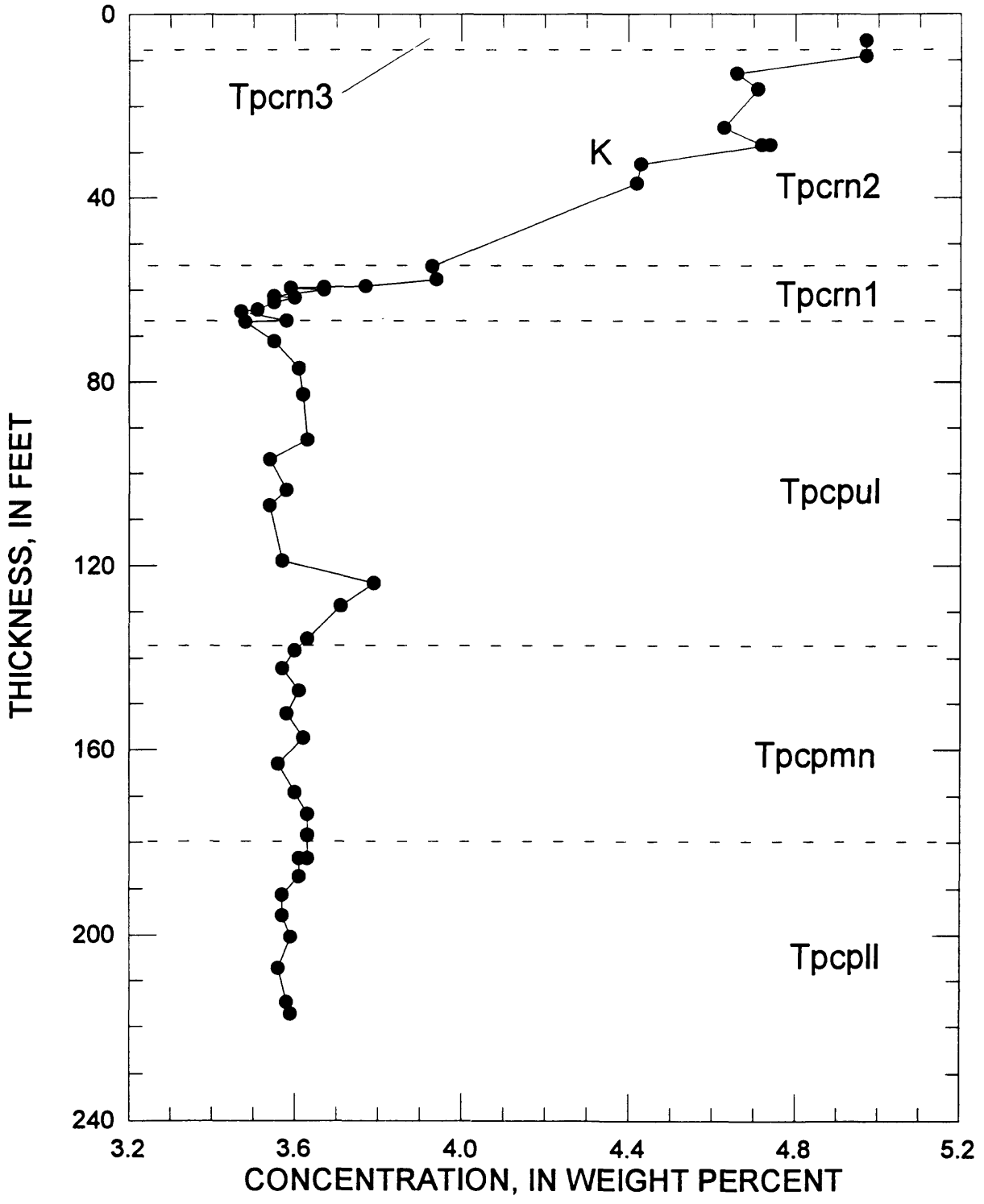

Figure 8. Concentrations of K in samples of the Tiva Canyon Tuff from drill hole UE-25 NRG#3.

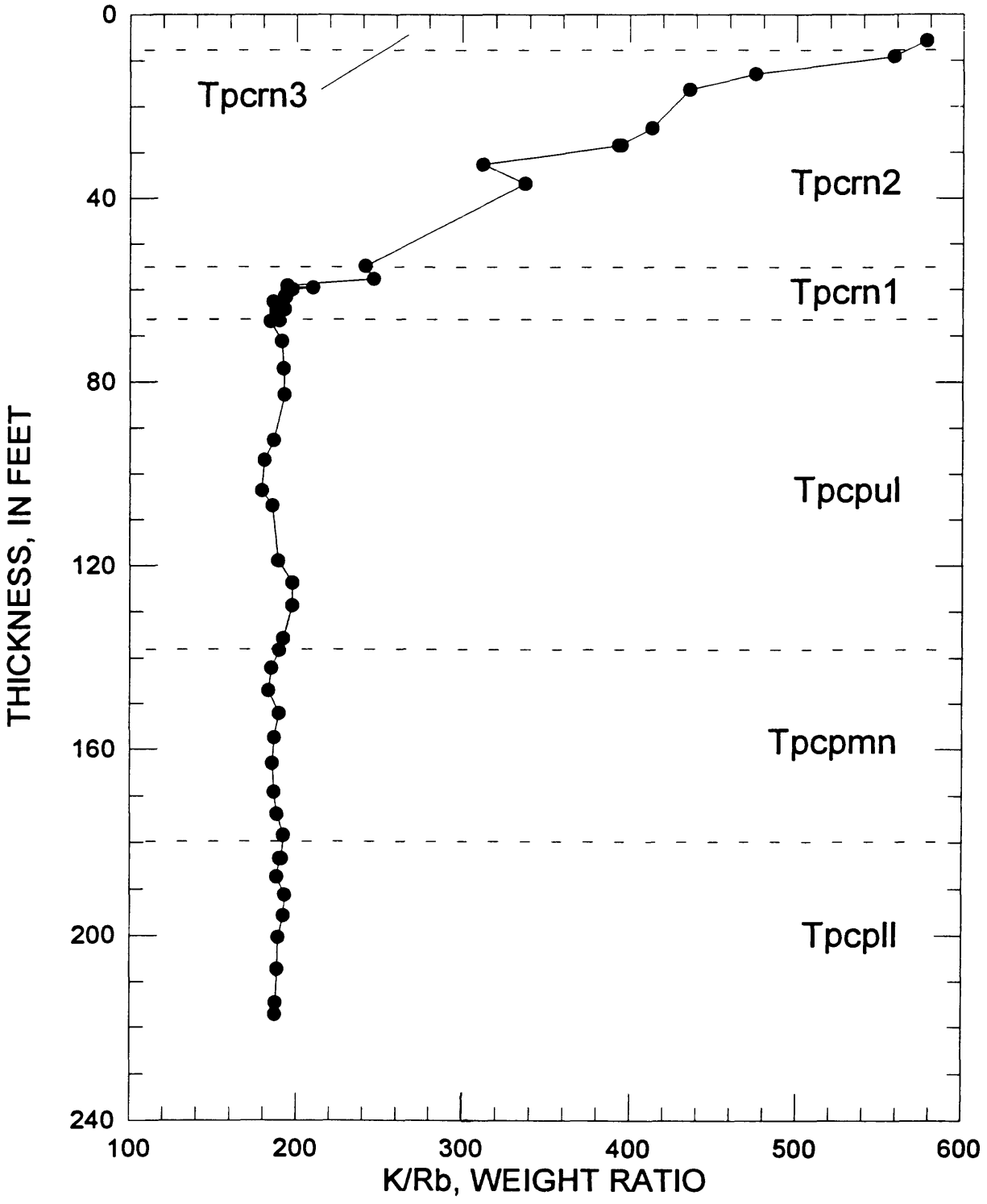

Figure 9. Variations of K/Rb ratio in samples of the Tiva Canyon Tuff from drill hole UE-25 NRG#3.

the unit, K/Rb ratios range from a mean of about 190 in the high-silica rhyolite to nearly 600 in the quartz latite of the pumice-poor subzone of the crystal-rich zone (table 1).

The strontium isotopic composition of the Tiva Canyon Tuff also varies systematically throughout the unit (fig. 10). The curve labelled "Present-day ratio" is defined by the measured $^{87}Sr/^{86}Sr$ ratios of the samples whereas the curve designated "Initial ratios" is the calculated initial $^{87}Sr/^{86}Sr$ ratios [IR (Sr)] assuming closed-system evolution from the depositional age of 12.7 Ma. The initial ratios for the high-silica rhyolite show limited variability with a mean of 0.7117. Unlike most of the geochemical trends, the IR(Sr) values do not change abruptly at the contact between the crystal-poor and crystal-rich zones but continue unchanged well into the crystal transition subzone followed by a sharp decrease to 0.7090 through the transitional quartz latite. These Sr-isotope variations are similar to those reported for bulk rock and sanidine samples of the Tiva Canyon Tuff by Farmer and others (1991).

In figure 11, data for a representative suite of samples of transitional quartz latite and quartz latite from NRG#3 have been normalized to the mean high-silica rhyolite (table 3). For each sample, element concentrations of individual samples are divided by the corresponding mean element concentrations of the high-silica rhyolite. The diagram emphasizes the progressive upward depletion in Rb and Nb, the remarkably constant Y, and the progressive enrichment in K, Ca, Ti, Sr, Zr, Ba, La, and Ce relative to the high-silica rhyolite.

The foregoing discussion emphasizes the geochemical similarity of the Tiva Canyon Tuff in NRG#3 with the samples from the Solitario Canyon, Whaleback Ridge, and Antler Ridge reference sections. These similarities include the general constancy of composition of the high-silica rhyolite in the crystal-poor zone, the sharp geochemical break between the crystal-poor and crystal-rich zones, the very significant increases in the concentrations of K, Ca, Sr, Zr, Ti, Ba, La, and Ce through the crystal-rich zone, and the decreases in Rb and Nb through the crystal-rich zone. However, two significant differences occur between the geochemical trends in samples from NRG#3 and those defined by the reference sections. In the reference sections, Ba, Ti, and Zr are excellent markers of the contact between the crystal-rich and crystal-poor zones. These elements also delineate the contact in NRG#3 (fig. 3), but the geochemical break is not as clear as in the reference sections because of reversals in concentrations in the lower part of the crystal-rich zone. A second clear distinction between NRG#3 and the reference sections is the rate of up-section element increase in the crystal-rich zone. For example, the variation in Ti can be approximated by a linear increase through the crystal-rich zone. In the Solitario Canyon, Antler Ridge, and Whaleback Ridge reference sections, Ti increases up section at 17 to 18 ppm per ft. In contrast, the increase through the crystal-rich zone in NRG#3 is 37 ppm per ft. Similarly, the rate of increase in Zr is 4.8 ppm per ft at Solitario Canyon, 5.5 at Whaleback, 5.3 and Antler, and 9.0 at NRG#3 or nearly twice that of the reference sections.

Unpublished data for samples from drill hole UE-25 NRG#2 provide possible further constraints on this apparent lateral geochemical variation in the crystal-rich zone of the Tiva Canyon Tuff. NRG#2 is located 685 ft east and 551 ft south of NRG#3. The vertical drill hole intercepted nonwelded tuffs and the vitric and crystal-rich zones of the Tiva Canyon Tuff (J. Geslin and T. Moyer, Science Applications International Corporation, written commun., 1993). After corrections are made for a 15° dip to the east, the stratigraphic thickness of the interval between the base of the pumice-poor subzone and the top of the crystal-rich zone is 72.9 ft. In NRG#3, this same interval is only 58.8 ft thick. The geochemical gradients in NRG#2 are 29 ppm Ti per ft and 7.2 ppm Zr per ft. These gradients are intermediate between those for the reference sections and for NRG#3. If the gradients in NRG#2 were compressed to reflect the stratigraphic thickness of the same interval in NRG#3, the calculated gradients would be 8.9 ppm Zr per ft and 36 ppm Ti per ft. The close agreement with the observed gradients in NRG#3 suggests that some part of the crystal-rich zone intercepted by the drill hole has been faulted out, resulting in the apparent compression of the geochemical gradients. Intersection of one or more west-dipping normal faults (west side down) by NRG#3 would result in apparent thinning of the unit. Assuming that the crystal-rich zone intercepted by NRG#2 has not been faulted, the integrated stratigraphic throw on the faults intercepted by NRG#3 would be 14 ft. NRG#3 is located close to the eastern side of a zone of closely spaced normal faults called the imbricate fault zone (Scott and Bonk, 1984). Thus, it is not unreasonable to postulate that NRG#3 inter-

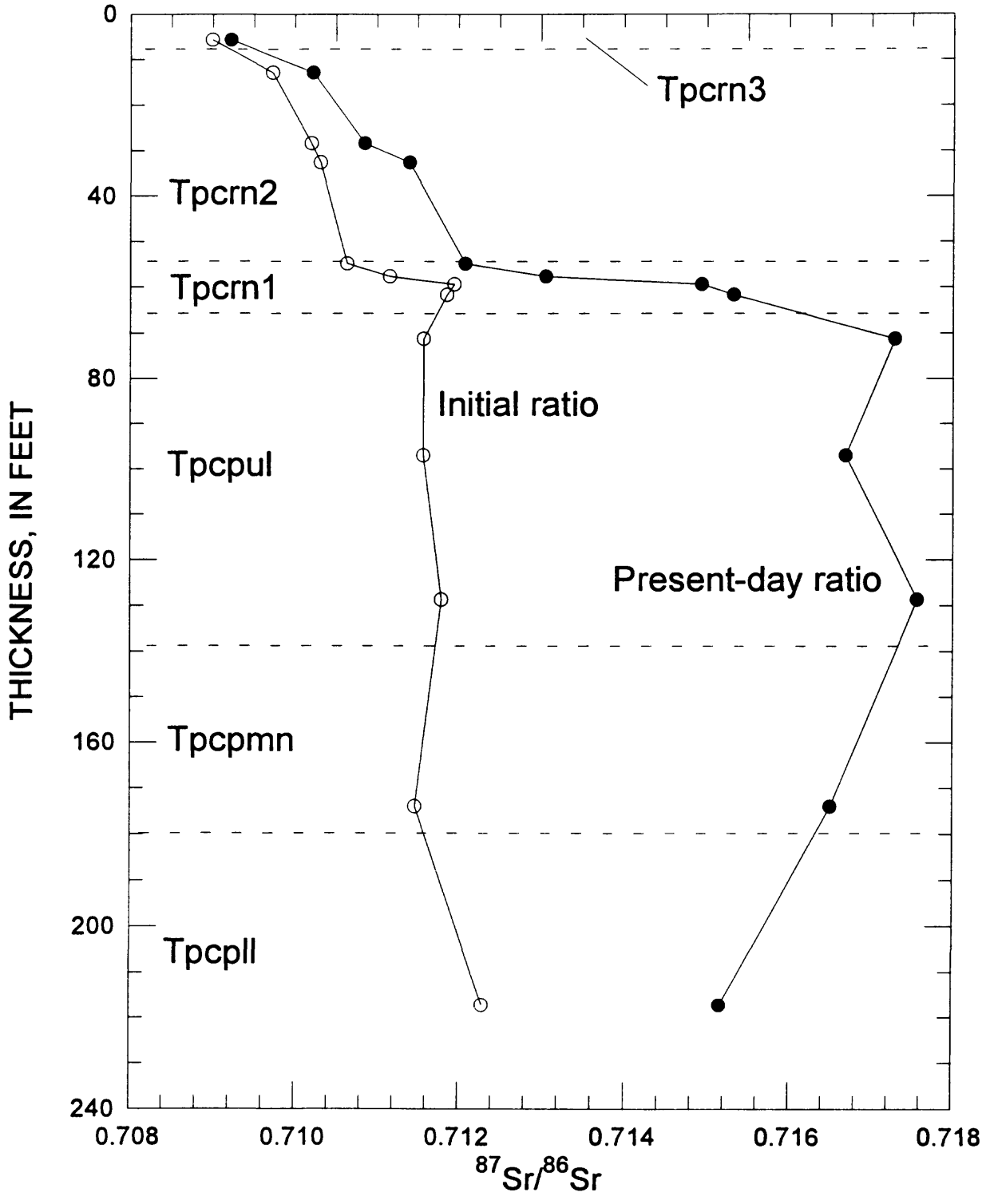

Figure 10. Variations of present-day and initial Sr-isotope ratios in samples of the Tiva Canyon Tuff from drill hole UE-25 NRG#3.

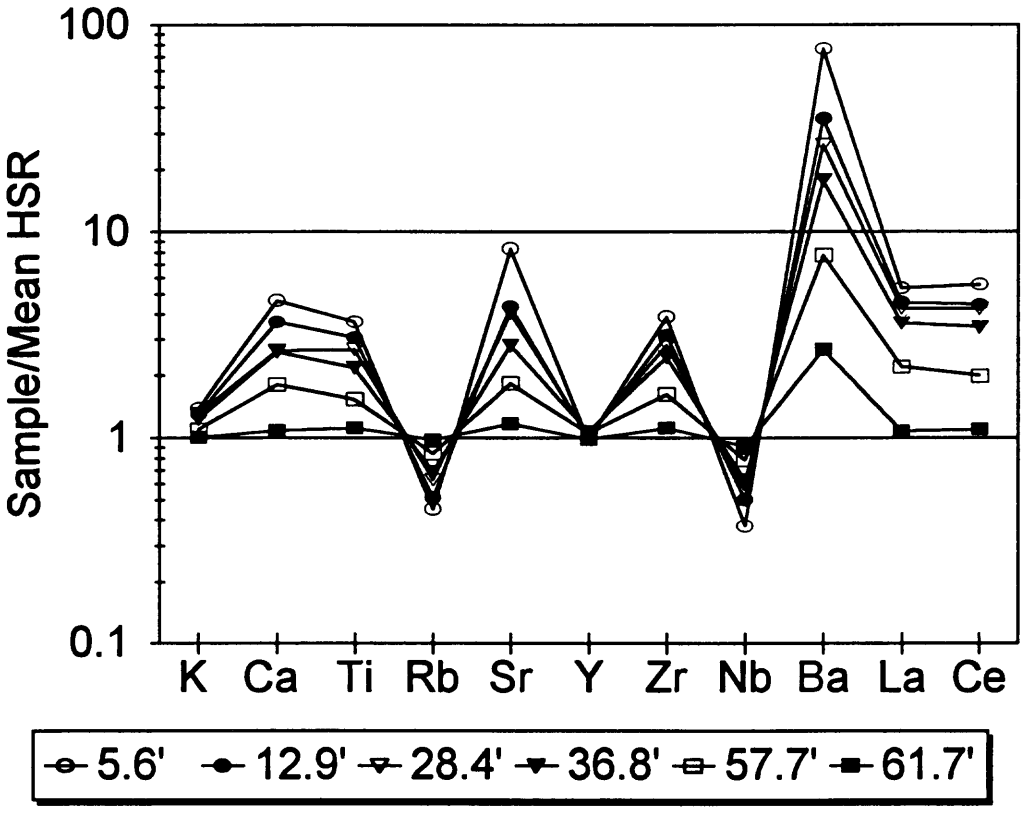

Figure 11. Comparison of element concentrations in selected samples of quartz latite with the mean values for high-silica rhyolite in UE-25 NRG#3.

sected one or more normal faults that cut out part of the crystal-rich zone along the alignment of the drill hole. The validity of this postulate can be tested in the ESF, which will have penetrated the Tiva Canyon Tuff close to both NRG#2 and NRG#3.

The observation of larger geochemical gradients in NRG#2 relative to those in the three reference sections also indicates a lateral change in these attributes, assuming that the section has not been faulted out along the drill hole. The existence of such lateral variations can be tested by establishing reference sections both east and west of the existing sections and drill holes. Use of the geochemical gradients to estimate stratigraphic throw along faults must consider these possible lateral changes in the gradients and rely on sections nearby the subject faults for reference.

SUMMARY

The distribution of the elements K, Ca, Ti, Rb, Sr, Y, Zr, Nb, Ba, La, and Ce in core samples of the Tiva Canyon Tuff from drill hole UE-25 NRG#3 at Yucca Mountain are similar to those observed in reference sections at Solitario Canyon, Whaleback Ridge, and Antler Ridge. Except for small differences, the high-silica rhyolite is laterally and vertically uniform in composition. The effects of alkali-element mobility have been observed in the lower vitric subzones of the Solitario Canyon reference section, but NRG#3 and the other reference sections do not intercept these lower subzones. The contact between the crystal-poor (high-silica rhyolite) and the crystal-rich (transitional quartz latite) zones is clearly identified geochemically in NRG#3, although some elements such as Ba and Ti show small-scale reversals in trend immediately above the contact.

The approximate monotonic increase in Ba, Zr, and Ti, especially, through the crystal-rich zone can be used to estimate stratigraphic throw along faults where zonal contacts are obscured. However, the rate of increase in these elements in NRG#3 is substantially larger than in the reference sections. Comparison of these trends and zonal thicknesses with those in

NRG#2, a nearby vertical hole that intercepts the crystal-rich zone of the Tiva Canyon Tuff, suggests the possibility that the intercepted crystal-rich zone at NRG#3 has had approximately 14 ft of section cut out by one or more normal faults. The rates of increase of elements stratigraphically upward in NRG#2 are also larger than those observed at the reference sections, which also suggests lateral variability in these attributes.

REFERENCES CITED

Broxton, D.E., Warren, R.G., and Byers, F.M., 1989, Chemical and mineralogic trends within the Timber Mountain-Oasis Valley caldera complex, Nevada—Evidence for multiple cycles of chemical evolution in a long-lived silicic magma system: Journal of Geophysical Research, v. 94, p. 5961–5985.

Buesch, D.C., Dickerson, R.P., Drake, R.M., and Spengler, R.W., 1994, Integrated geology and preliminary cross section along the north ramp of the Exploratory Studies Facility, Yucca Mountain: Fifth International Conference on High Level Radioactive Waste Symposium, v. 2, p. 1055–1065.

Byers, F.M., Jr., Orkild, P.P., Quinlivan, W.D., and Sargent, K.A., 1976, Volcanic suites and related cauldrons of Timber Mountain-Oasis Valley caldera complex, southern Nevada: U.S. Geological Survey Professional Paper 919, 70 p.

Cas, R.A.F., and Wright, J.V., 1993, Volcanic successions—Modern and ancient: London, Chapman and Hall, 528 p.

Farmer, G.L., Broxton, D.E., Warren, R.G., and Pickthorn, W., 1991, Nd, Sr, and O isotopic variations in the metaluminous ash-flow tuffs and related volcanic rocks at the Timber Mountain/Oasis Valley caldera complex, SW Nevada—Implications for the origin of large-volume silicic magma bodies: Contributions to Mineralogy and Petrology, v. 109, p. 53–68.

Flood, T.P., Vogel, T.A., Schuraytz, B.C., 1989, Chemical evolution of a magmatic system—The Paintbrush Tuff, southwest Nevada volcanic field: Journal of Geophysical Research, v. 94, p. 5943–5960.

Geslin, J.K., Moyer, T.C., and Buesch, D.C., 1995, Summary of lithologic logging of new and existing boreholes at Yucca Mountain, Nevada—August 1993 to February 1994: U.S. Geological Survey Open-File Report 94-342, 39 p.

Hildreth, W., 1981, Gradients in silicic magma chambers—Implications for lithospheric magmatism: Journal of Geophysical Research, v. 86, p. 10153–10192.

Johnson, C.M., 1989, Isotopic zonations in silicic magma chambers: Geology, v. 17, p. 1136–1139.

Lipman, P.W., 1965, Chemical comparison of glassy and crystalline volcanic rocks: U.S. Geological Survey Bulletin 1201-D, p. D1–D24.

Lipman, P.W., Christiansen, R.L., and O'Connor, J.T., 1966, A compositionally zoned ash-flow sheet in southern Nevada: U.S. Geological Survey Professional Paper 524-F, p. F1–F47.

Marshall, B.D., Kyser, T.K., and Peterman, Z.E., in press, Oxygen isotopes and trace elements in the Tiva Canyon Tuff, Yucca Mountain and vicinity, Nye County, Nevada: U.S. Geological Survey Open-File Report 95-431.

Noble, D.C., and Hedge, C.E., 1969, $^{87}Sr/^{86}Sr$ variations within individual ash-flow sheets: U.S. Geological Survey Professional Paper 650-C, p. C133–C139.

Peterman, Z.E., Spengler, R.W., Futa, K., Marshall, B.D., and Mahan, S.A., 1991, Assessing the natural performance of felsic tuffs using the Rb-Sr and Sm-Nd systems—A study of the altered zone in the Topopah Spring Member, Paintbrush Tuff, Yucca Mountain, Nevada *in* Scientific Basis for Nuclear Waste Management XIV, Pittsburgh, Penn., Materials Research Society, p. 687–694.

Schuraytz, B.C., and Vogel, T.A., 1989, Evidence of dynamic withdrawal from a layered magma body—The Topopah Spring Tuff, southwestern Nevada: Journal of Geophysical Research, v. 94, p. 5925–5942.

Scott, R.B., and Bonk, J., 1984, Preliminary geologic map of Yucca Mountain, Nye County, Nevada, with geologic sections: U.S. Geological Survey Open-File Report 84-494, scale 1:12,000.

Singer, F.R., Byers, F.M., Jr., Widmann, B.L., Dickerson, R.P., 1994, Petrographic and geochemical characteristics of a section through the Tiva Canyon Tuff at Antler Ridge, Yucca Mountain, Nevada *in* High Level Radioactive Waste Management, Proceedings of the 5th International Conference, Las Vegas, Nev., 1994, La Grange Park, Ill., American Nuclear Society and American Society of Civil Engineers, p. 1869–1879.

Smith, R.L., 1979, Ash-flow magmatism *in* Chapin, C.E., and Elston, W.E., eds., Ash-flow tuffs: Geological Society of America Special Paper 180, p. 5–27.

Tegtmeyer, K.J., and Farmer, G.L., 1990, Nd isotopic gradients in upper crustal magma chambers—Evidence for in situ magma-wall-rock interaction: Geology, v. 18, p. 5–9.

☆ U.S. GOVERNMENT PRINTING OFFICE: 1996 - 774-216 / 00098 REGION NO. 8